Computational Materials Science 92 (2014) 451–456

Contents lists available at ScienceDirect

Computational Materials Science

journal homepage: www.elsevier.com/locate/commatsci

Electronic and optical properties of MoS_2–WS_2 multi-layers: First principles study

Ushma Ahuja [a], Alpa Dashora [b,*], Harpal Tiwari [c], Dushyant C. Kothari [b], K. Venugopalan [d]

[a] Faculty of Engineering, M.L. Sukhadia University, Udaipur 313 001, Rajasthan, India
[b] Department of Physics and National Centre for Nanosciences & Nanotechnology, University of Mumbai, Vidyanagri, Santacruz (E), Mumbai 400 098, Maharashtra, India
[c] Department of Electrical Engineering, Malaviya National Institute of Technology, Jaipur 302 017, Rajasthan, India
[d] Department of Physics, M.L. Sukhadia University, Udaipur 313 001, Rajasthan, India

ARTICLE INFO

Article history:
Received 9 April 2014
Received in revised form 30 May 2014
Accepted 5 June 2014
Available online 9 July 2014

Keywords:
Electronic structure
Photovoltaics
Metal dichalcogenides
Optical properties

ABSTRACT

MoS_2–WS_2 thin layers with different deposition sequences and stacking configurations have been studied using first principles full potential linearized augmented plane wave method. The electronic and optical properties of ten atomic layers (in [0001] direction) of MoS_2–WS_2 are reported in the present paper. Ten layers of MoS_2–WS_2, which are free from quantum size effects, show an indirect band gap which varies between 0.89 and 1.22 eV by engineering of the layering sequence and stacking configuration. Optical properties like absorption coefficients, dielectric tensors and refractive indices of bilayer and multilayer films of MoS_2–WS_2 are determined and are found to be different from the ten layers of MoS_2 and WS_2. Changes in the electronic and optical properties of multilayers have been elaborated in terms of interlayer and intralayer S–S distances. A comparison of absorption spectra deduced using the first principles calculations for Si and different combinations of multilayers of MoS_2–WS_2 show their applicability in optoelectronics and photovoltaic devices.

1. Introduction

Engineering of band gap by devising a hetero-junction of two semiconductors is a very promising technique in semiconductor science and technology for its use in important applications, such as solar cells, electronic and optoelectronic devices, and radiation detectors [1,2]. With the rise of 2D semiconductor technology and recent advances in thin film preparation, exfoliation technique, optical detection, transfer and manipulation of 2D materials, etc., the idea of exploration of new genres of physics has generated a lot of interest among scientists and engineers [3]. In this scenario, first principles calculations play a very crucial role in introducing new materials which can motivate and give new ideas to experimentalists whilst reducing the experimental efforts.

Within the last few years, new 2D layered compounds like graphene, h-BN, layered transition metal dichalcogenides (TX_2, where T is the transition metal and X is the chalcogen atom) have been studied for their roles in semiconductor device applications [4]. In these layered compounds, electronic properties drastically change with changes in thickness and structure of layers. In the case of graphene, many authors have studied the stacking effects and subsequent changes in the band gap both experimentally and theoretically [5,6]. Effect of vertical electric field on the electronic properties of multilayer graphene has been studied by Kumar and Guo [7]. Similar studies on h-BN are also present in the literature [8–10]. Few attempts have also been made to explore the graphene/h-BN interfaces [11–13]. Due to an analogy in structure with graphene, TX_2 films have attracted several workers for their thickness-dependent electronic properties [14–16].

MoS_2 and WS_2 belong to the same family of TX_2 compounds. Both the MoS_2 and WS_2 compounds have an indirect band gap in bulk form which changes to a direct band gap when they are thinned to a monolayer [17–19]. The lattice parameters of both the compounds are almost similar which envisions intriguing electronic properties in the mixed compound [20]. Strong dependence of band-offset on number of layers in TX_2 (T = Mo, W; X = S, Se, Te) hetero-structures have been studied by Kang et al. [21] using Vienna ab-initio simulation package (VASP). The authors have discussed their suitability in optoelectronics and energy conversion, etc. Kou et al. [22] have reported nanostructured $(MoX_2)_n(MoY_2)_m$ (X, Y = S, Se or Te) hetero-structures by employing density functional theory (DFT) and reported a considerable change in the band gap by changing the composition and thickness as well as by applying an electric field. Optical and electronic properties of thin films of ternary mixed dichalcogenides $[Mo(S_{1-x}Se_x)_2]$ have been

* Corresponding author. Tel.: +91 86 5588 4986; fax: +91 22 2652 8835.
E-mail address: dashoralpa@gmail.com (A. Dashora).

http://dx.doi.org/10.1016/j.commatsci.2014.06.005
0927-0256/

studied by Ajalkar et al. [23]. They observed a decrement in band gap of the mixed dichalcogenides on increasing the concentration of Se. Komsa and Krasheninnikov [24] have explored the electronic properties of a single layer of $MoS_{2x}Se_{2(1-x)}$. They reported benefits of this mixed bilayer 2D compound for optoelectronic applications. Thermoelectric properties of TX_2 on layer mixing have been explored by Lee et al. [25] using DFT. Lopez-Sanchez et al. [26] have reported a design of ultrasensitive monolayer MoS_2 phototransistor, with improved device mobility and ON current. Recently on the basis of DFT and GW-Bethe Salpeter method, Bernardi et al. [27] have shown that monolayers of MoS_2, $MoSe_2$ and WS_2 (with thickness $\leqslant$1 nm) can absorb 5–10% of incident sunlight which is higher than absorption by GaAs and Si. Therefore, it is of keen interest to investigate the effect of MoS_2 and WS_2 interfaces on the electronic and optical properties of these mixed dichalcogenides with different layer and stacking arrangements.

In this paper, using full potential linearized augmented plane wave (FP-LAPW) method, we report the electronic and optical properties of ten atomic layers (in [0001] direction) of MoS_2, WS_2 and MoS_2–WS_2 with varying sequences in layer deposition and two different stacking configurations namely, AB and AA as shown in Fig. 1(a–d). In the AB stacked MoS_2 (WS_2), the Mo (W) atom of the upper layer sits directly above the S atom of the lower layer. To check the geometry-induced effect on the interlayer interaction and electronic properties, we also consider the AA stacking configuration in which the Mo (W) atoms of the upper layer sit right above the Mo (W) atoms of the lower layer. We also discuss the effect of interlayer and intralayer S–S distances on the electronic properties of the mixed chalcogenides and their constituents namely, MoS_2 and WS_2. In the major energy range of the solar spectrum, absorption coefficients of layers of MoS_2–WS_2 are compared to that of bulk Si to explore the feasibility of these layers for photovoltaic applications.

2. Theoretical methodology

The present calculations have been performed using FP-LAPW method as embodied in Wien2k code [28]. The FP-LAPW method allows a better description of the rapidly changing wave functions, potentials and electron density close to the nuclei as well as the smoother part of these quantities in between the atoms. In the present study, we have used modified Becke–Johnson (mBJ) potential [29] within generalized gradient approximation (GGA) [30]. It is known that the mBJ-GGA overcomes the well-known problem of underestimation of band gap by employing DFT. We have taken lattice parameters as 3.16 Å and 3.15 Å for MoS_2 and WS_2 layers, respectively [15]. By constructing the super cell in z-direction, we have generated non-polar layers of MoS_2 and WS_2 in form of ten atomic layers along the [0001] direction with a vacuum of 25 Å. Throughout this paper, we have addressed these layers as $(MoS_2)_{10L}$ and $(WS_2)_{10L}$, where the subscript L stands for layers. To check the MoS_2 and WS_2 interface effect, we have also generated bilayered $(MoS_2)_{5L}$–$(WS_2)_{5L}$ and multilayered $(MoS_2$–$WS_2)_{5L}$ arrangement (Fig. 1b and c). It may be noted that the $(MoS_2)_{5L}$–$(WS_2)_{5L}$ arrangement corresponds to five layers of MoS_2 on top of five layers of WS_2, while the $(MoS_2$–$WS_2)_{5L}$ corresponds to alternate monolayers of MoS_2 and WS_2 repeated five times. All the AA and AB stacked $(MoS_2)_{10L}$, $(WS_2)_{10L}$, $(MoS_2)_{5L}$–$(WS_2)_{5L}$ and $(MoS_2$–$WS_2)_{5L}$ layers were fully relaxed for atomic forces until the forces on each atom reach a value less than 5 mRy per atomic unit (a.u.). To ensure sufficient accuracy in convergence, total energy of the layers was converged to 0.01 mRy.

It is worth mentioning that the radius of Muffin Tin (MT) spheres for Mo and W was set as 2.41 a.u. while for S it was set as 2.13 a.u. For all the layers, the ***k***-point integration over the irreducible Brillouin zone (IBZ) was performed using a mesh of $10 \times 10 \times 1$ ***k***-points. Values of other governing parameters such as cut-off for charge density (G_{max}), maximum radial expansion (l_{max}) and $R_{MT}K_{max}$ were kept as 12, 10 and 7, respectively. To compare the optical properties of the studied layers with that of bulk Si, we have also computed the electronic and optical properties of Si using the FP-LAPW calculations (with G_{max} = 12, l_{max} = 10, $R_{MT}K_{max}$ = 7 and $10 \times 10 \times 10$ ***k***-points in the IBZ).

The difference in total energy between AB and AA stacking configurations was observed to be less than 0.07 Ry/atom for all the layers. Since AB stacking leads to the lowest total energy, they are found to be more stable than AA stacking. For MoS_2–WS_2 interfaces, the present computations also predict that the $(MoS_2$–$WS_2)_{5L}$ arrangement is energetically more preferred than $(MoS_2)_{5L}$–$(WS_2)_{5L}$ layers.

For computation of optical properties within the Wien2k code [28], we have used the formulation suggested by Draxl and Sofo

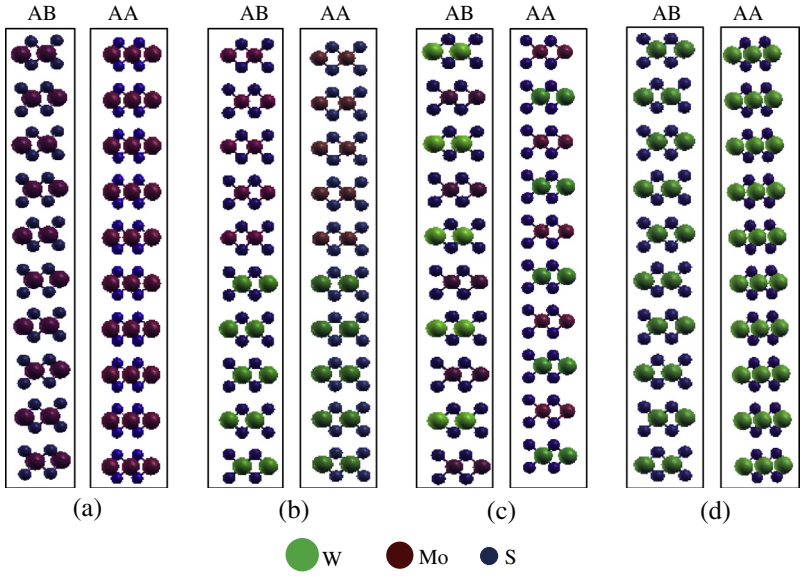

Fig. 1. Atomic arrangement in multilayers corresponding to (a) $(MoS_2)_{10L}$, (b) $(MoS_2)_{5L}$–$(WS_2)_{5L}$, (c) $(MoS_2$–$WS_2)_{5L}$ and (d) $(WS_2)_{10L}$ systems with AB and AA stacking sequences. The multilayers correspond to [0001] direction. Vacuum (25 Å) at both the ends of 10 layers are not shown.

[31]. To compute the various optical properties, we have considered 300 unoccupied states for all the studied layers. Lorentz broadening of 0.1 eV was applied to all the optical spectra.

3. Results and discussion

In Fig. 2(a–d), we have presented the energy bands for $(MoS_2)_{10L}$, $(MoS_2)_{5L}$–$(WS_2)_{5L}$, $(MoS_2$–$WS_2)_{5L}$ and $(WS_2)_{10L}$ layers with AB (left panel) and AA (right panel) stacking configurations. The corresponding density of states (DOS) for all the layers with both types of stacking have been presented in Fig. 3(a and b). From Fig. 2(a and b) it is visible that all the layers show an indirect band gap between Γ point and Γ–K branch of BZ. The overall topology of energy bands in all the layers is similar except the energy range and dispersion of bands at a few points of BZ. In the case of $(MoS_2)_{5L}$–$(WS_2)_{5L}$ and $(MoS_2$–$WS_2)_{5L}$ (Fig. 2(b and c), left panel), it is found that the lower valence bands (below −6.0 eV) at Γ point shift to lower and higher energy sides respectively and disperse more in comparison to $(MoS_2)_{10L}$ and $(WS_2)_{10L}$. $(MoS_2$–$WS_2)_{5L}$ layer with AB stacking shows a higher number of degenerate bands in valence and conduction region at M and K points. A major change is observed in the lower conduction region which is dominated by Mo and W states, as shown in Fig. 3(a). The 5d states of W are found to form energy bands at energy values higher than those of Mo 4d states (partial DOS are not shown here). In the low conduction bands, difference of about 0.5 eV between DOS of Mo-4d and W-5d in $(MoS_2)_{5L}$–$(WS_2)_{5L}$ and $(MoS_2$–$WS_2)_{5L}$ environment is found, as can be seen in Fig. 3(a). In the case of $(MoS_2$–$WS_2)_{5L}$ (Fig. 2(c), left panel) the parallel bands in general are confined in a narrow region. The configuration of stacking also affects the energy bands considerably as depicted for the AA arrangement in the right hand side panel of Fig. 2(a–d). AA stacking reduces the degeneracy of bands mainly in the upper valence band (between 0.0 and −5.5 eV) and in the conduction bands mainly at M and K points of the BZ as seen in Fig. 2(a–d).

In Table 1, we have collated the variation of band gap deduced from valence band maximum (at Γ point) and conduction band minimum (in Γ–K branch) for all the studied layers. It can be seen that in both the stacking configurations, the indirect band gap of $(WS_2)_{10L}$ remains higher than that of $(MoS_2)_{10L}$. It is observed that the band gaps in MoS_2–WS_2 interfaces strongly depend on the arrangement of layers and stacking configurations. In the case of $(MoS_2$–$WS_2)_{5L}$ arrangement with AB stacking, the indirect band gap (1.22 eV) is higher than the band gap of $(MoS_2)_{10L}$ (1.07 eV) while a reverse trend is seen for $(MoS_2)_{5L}$–$(WS_2)_{5L}$ arrangement with a 0.97 eV band gap. We observed that a change in stacking configuration from AB → AA in MoS_2–WS_2 layers reduces the band gap. Computed direct band gaps for AA and AB stacked layers at special $\boldsymbol{k}$-points of the BZ are also collated in Table 1. We have also included the band gaps of bulk MoS_2, WS_2 and Si which have been computed using mBJ-GGA in Table 1. Since the mBJ-GGA based band gap of bulk compounds is close (within 10%) to their corresponding experimental values [32,33], it validates the reliability of band gap calculations of multilayers reported in this paper.

Owing to different stacking configurations and layer deposition sequences in the studied layers, apart from the changes in the band gap, interlayer and intralayer interactions are also expected to vary. In Table 2, we have shown the interlayer and intralayer S–S distances (in vertical direction) as deduced from the present FP-LAPW calculations. In the AB stacked $(MoS_2)_{10L}$, the intralayer

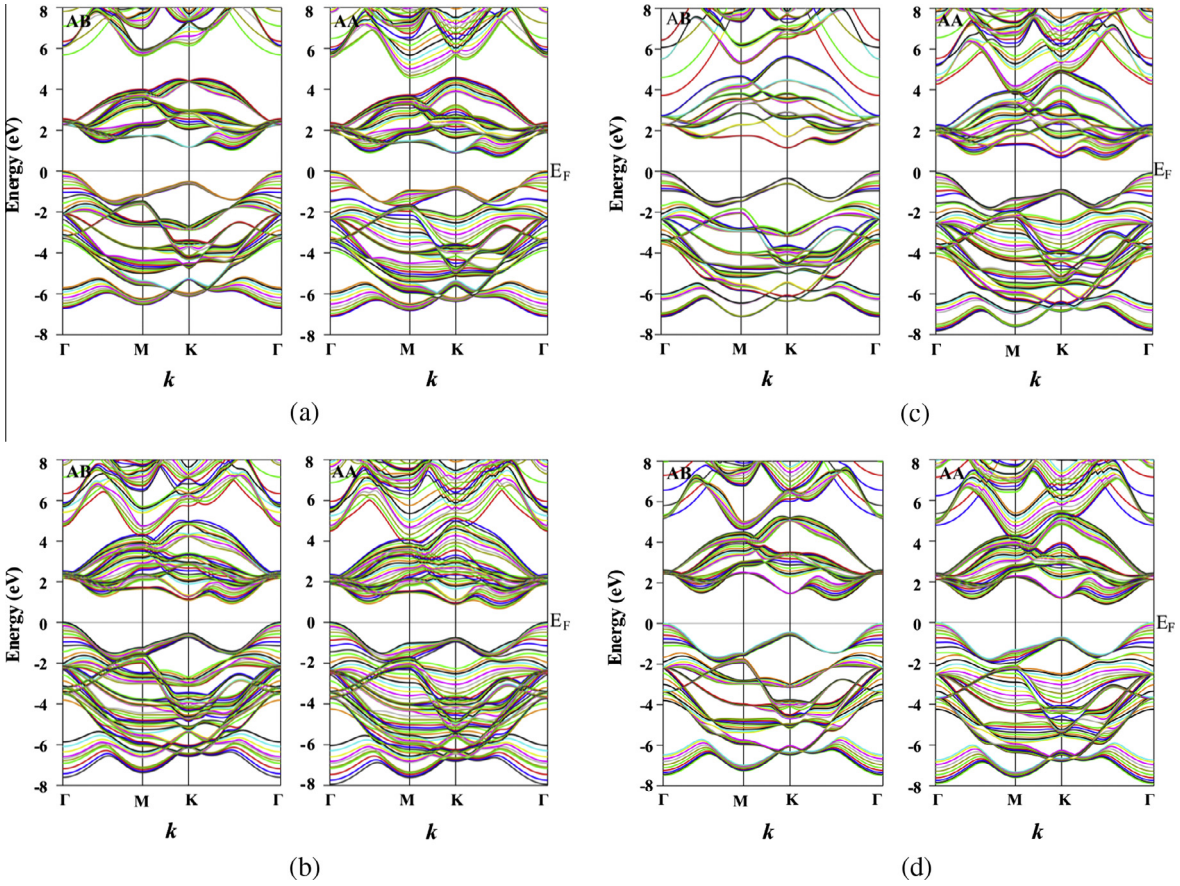

Fig. 2. Energy band (E–$\boldsymbol{k}$) diagrams for (a) $(MoS_2)_{10L}$, (b) $(MoS_2)_{5L}$–$(WS_2)_{5L}$, (c) $(MoS_2$–$WS_2)_{5L}$ and (d) $(WS_2)_{10L}$ thin films with AB (left panel) and AA (right panel) stacking configurations.

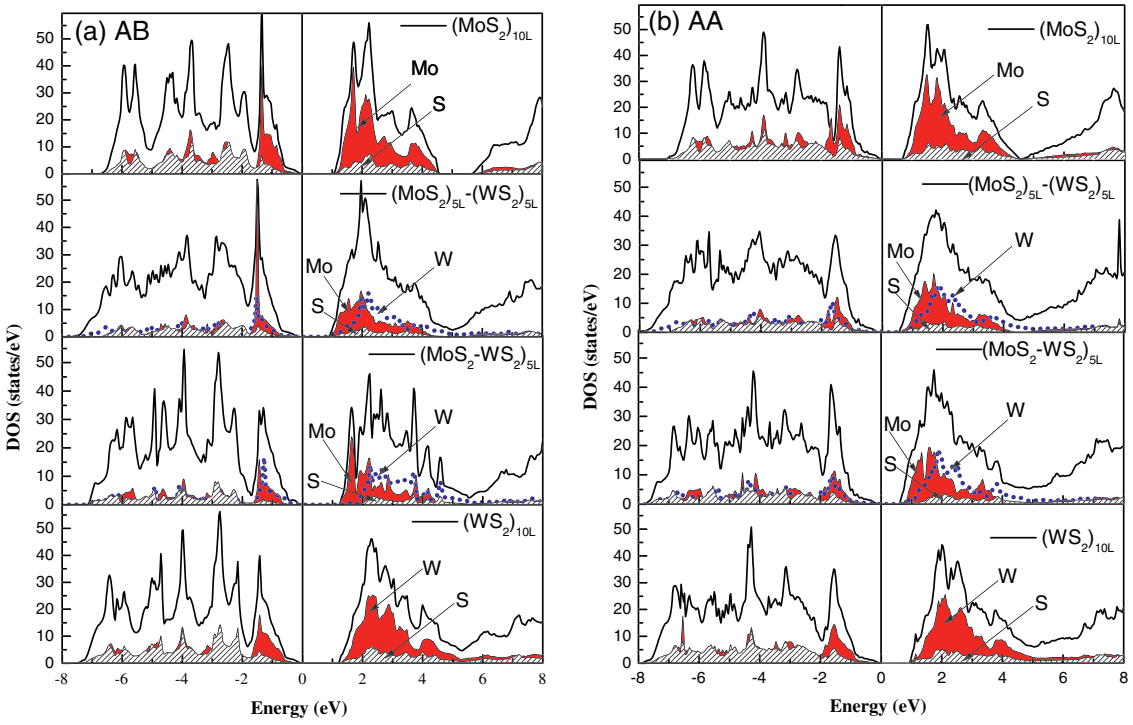

Fig. 3. Total and partial density of states for (a) AB and (b) AA stacking of $(MoS_2)_{10L}$, $(MoS_2)_{5L}$–$(WS_2)_{5L}$, $(MoS_2$–$WS_2)_{5L}$ and $(WS_2)_{10L}$ multilayers.

Table 1
Indirect and direct band gap in $(MoS_2)_{10L}$, $(MoS_2)_{5L}$–$(WS_2)_{5L}$, $(MoS_2$–$WS_2)_{5L}$ and $(WS_2)_{10L}$ multilayers with AB and AA stacking configurations along with bulk MoS_2, WS_2 and Si.

Layer/stacking arrangement	Indirect band gap		Direct band gap					
	Between Γ point and Γ–K branch		At Γ point		At M point		At K point	
	AB	AA	AB	AA	AB	AA	AB	AA
$(MoS_2)_{10L}$	1.07	0.71	2.27	1.88	2.88	2.64	1.86	2.35
$(MoS_2)_{5L}$–$(WS_2)_{5L}$	0.97	0.89	2.16	1.86	2.89	2.68	1.62	1.84
$(MoS_2$–$WS_2)_{5L}$	1.22	0.91	2.28	2.14	3.01	2.83	1.48	1.79
$(WS_2)_{10L}$	1.29	0.99	2.44	2.11	3.91	3.55	1.90	1.89
Bulk MoS_2	1.10, 1.23 [32]		2.13		2.92		1.75	
Bulk WS_2	1.30, 1.35 [32]		2.43		4.01		1.95	
Bulk Si	1.11[a], 1.13 [33]		3.11		3.97[b]		3.29[c]	

[a] Indirect band gap between Γ point and Γ–X branch.
[b] Direct band gap at X point.
[c] Direct band gap at L point.

Table 2
Interlayer and intralayer S–S distances in $(MoS_2)_{10L}$, $(MoS_2)_{5L}$–$(WS_2)_{5L}$, $(MoS_2$–$WS_2)_{5L}$ and $(WS_2)_{10L}$ multilayers with AB and AA stacking configurations.

Arrangement of layers and stacking		S–S distance (Å)	
		Intralayer	Interlayer
$(MoS_2)_{10L}$	AB	3.17	3.49
	AA	3.14	3.01
$(MoS_2)_{5L}$–$(WS_2)_{5L}$	AB	3.14	3.50
	AA	3.14	3.00
$(MoS_2$–$WS_2)_{5L}$	AB	3.14	3.51
	AA	3.12	3.03
$(WS_2)_{10L}$	AB	3.18	3.49
	AA	3.16	3.02

S–S distance is calculated to be 3.17 Å while the interlayer S–S distance comes out to be 3.49 Å. In comparison to the AB stacked arrangement, a very small reduction (0.03 Å) in the intralayer S–S distance is observed in the AA configuration. The interlayer S–S distance in AA stacking of $(MoS_2)_{10L}$ is found to be much smaller than that in AB stacking. Similarly in all the other films, the interlayer S–S distance is found to be lower in AA stacking than the AB arrangement. Therefore, a weaker interlayer interaction in AB stacking, in comparison to the intralayer interaction, is expected. The difference in interactions is supposed to play a major role in the electronic properties of these layers.

In Fig. 4(a and b), we have plotted the frequency dependent absorption coefficient (average) of all the layers with AB and AA stacking configurations along with standard solar spectrum [34]. The average value is deduced from the parallel and perpendicular components of the absorption coefficients. Both the stacking configurations show differences in absorption coefficients of the multilayers. From Fig. 4, it can be seen that most of the intense part of radiations received from the sun lies in the energy range 0.5–5.0 eV. Absorption coefficients for all the studied multilayer arrangements show almost zero absorption below 2.0 eV. The integrated intensities of absorption coefficients (area under the absorption curves) deduced from Fig. 4 for energy ranges 2.0–3.5 eV and 3.5–5.0 eV are compiled in Table 3. Two different energy

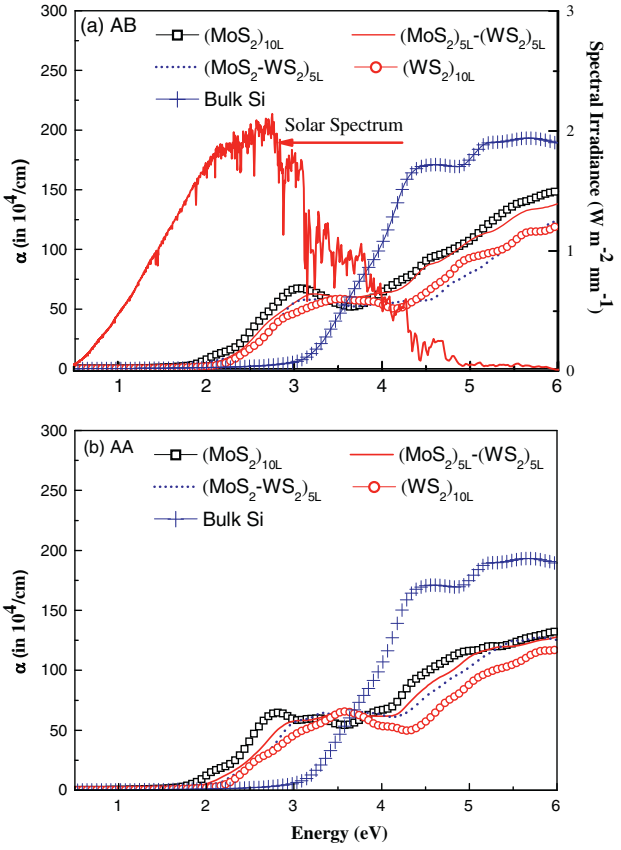

Fig. 4. Variations of absorption coefficients of $(MoS_2)_{10L}$, $(MoS_2)_{5L}$–$(WS_2)_{5L}$, $(MoS_2$–$WS_2)_{5L}$ and $(WS_2)_{10L}$ multilayers with (a) AB and (b) AA stacking configurations. Also included here is the absorption coefficient for bulk Si as calculated using FP-LAPW method. Intensity of solar spectra [34] is also shown at the scale marked in the right hand side.

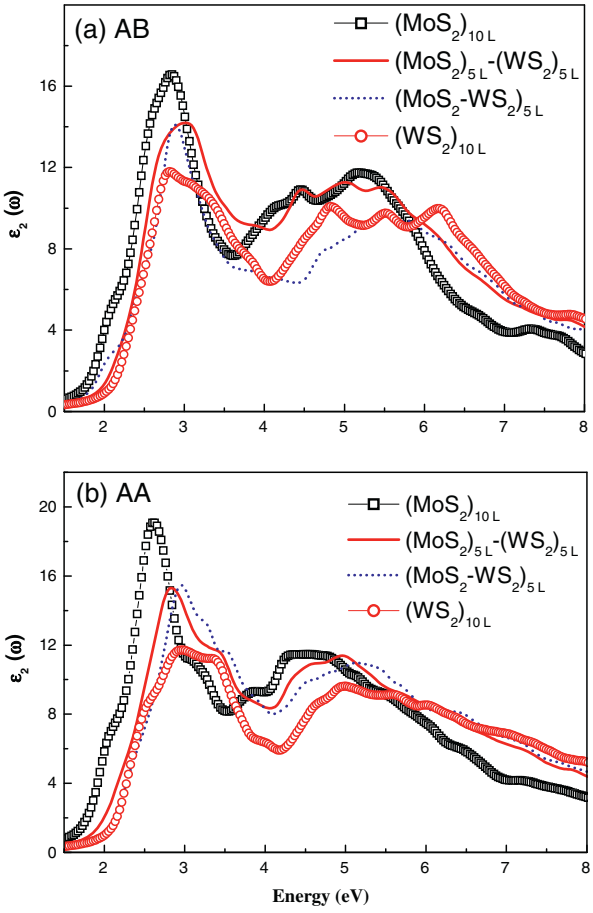

Fig. 5. Imaginary part of dielectric tensor of $(MoS_2)_{10L}$, $(MoS_2)_{5L}$–$(WS_2)_{5L}$, $(MoS_2$–$WS_2)_{5L}$ and $(WS_2)_{10L}$ multilayers with (a) AB and (b) AA stacking configurations.

regions (2.0–3.5 eV and 3.5–5.0 eV) have been considered as in the energy range of 2.0–3.5 eV, the absorption spectra of Si is lower than the absorption spectra of studied multilayers. On the other hand, in the range 3.5–5.0 eV, wherein the solar intensity is small, Si shows higher absorption than the studied multilayers (Fig. 4a). The integrated absorption for different layer arrangements and stacking configurations in the energy range of 2.0–3.5 eV shows that absorption for AB or AA stacking in different layers is about four to five times higher than that for bulk Si. While in higher energy range (3.5–5.0 eV), integrated absorption of all the multilayers is lower than that of Si. For solar applications, AB stacking configuration may be preferred in these multilayers owing to its stability. It is worth noting that Lee et al. [25] have predicted the strong enhancement of thermoelectric properties in similar type of mixed layered compounds. On combining investigations of Lee et al. [25] and the present data, we suggest use of MoS_2–WS_2 multilayers in the forthcoming optoelectronics and photovoltaic devices.

In Fig. 5(a and b), we have shown the averaged imaginary part of dielectric tensor $\varepsilon_2(\omega)$ for all the multilayers. Broad peaks between 2 and 3 eV in all the multilayers are well justified by the direct transitions between the S-p states (valence band maximum) and Mo-d states (conduction band minimum) at Γ and M points. It is worth mentioning that such transitions follow the

Table 3
Integrated absorption coefficients along with perpendicular and parallel components of dielectric constant and refractive index of $(MoS_2)_{10L}$, $(MoS_2)_{5L}$–$(WS_2)_{5L}$, $(MoS_2$–$WS_2)_{5L}$ and $(WS_2)_{10L}$ multilayers with AB and AA stacking and those for bulk Si, MoS_2 and WS_2.

S. no.	Arrangement of layers and stacking		Integrated absorption coefficient ($\times 10^4$/cm)		Dielectric constant		Refractive index	
			2.0–3.5 eV	3.5–5.0 eV	$\varepsilon_{1\perp}(0)$	$\varepsilon_{1\parallel}(0)$	$n_\perp(0)$	$n_\parallel(0)$
1	$(MoS_2)_{10L}$	AB	67.86	129.50	12.15	7.55	3.49	2.75
		AA	69.54	125.21	12.60	8.31	3.55	2.88
2	$(MoS_2)_{5L}$–$(WS_2)_{5L}$	AB	59.99	115.73	11.74	7.69	3.42	2.77
		AA	63.31	112.31	11.82	8.14	3.43	2.85
3	$(MoS_2$–$WS_2)_{5L}$	AB	60.28	115.82	10.45	6.41	3.24	2.65
		AA	62.58	113.25	11.50	7.72	3.39	2.78
4	$(WS_2)_{10L}$	AB	51.20	107.11	10.43	6.86	3.23	2.62
		AA	52.94	105.65	10.59	6.98	3.25	2.64
5	Bulk Si		12.11	195.60	9.89	9.89	3.15	3.15
6	Bulk MoS_2				15.79, 12.80 [37]	10.12, 8.90 [37]	3.97	3.18
7	Bulk WS2				12.82, 11.70 [37]	8.21, 8.70 [37]	3.58	2.86

dipole selection rule which dictates that only the transitions changing the angular momentum quantum number (Δl) by unity (± 1) are allowed. Generally, peaks in $\varepsilon_2(\omega)$ for the AA stacked multilayers (Fig. 5b) are found to be sharper than those in the AB stacking, which is attributed to lower band gap in the AA stacked multilayers than in the AB arrangement.

In Table 3, we have also collated the optical constants namely, real part of dielectric constant, $\varepsilon_1(0)$, and refractive index, n(0), in parallel and perpendicular directions of the incident radiations for all the studied multilayers, bulk Si, MoS_2 and WS_2. In all the studied multilayers, significant anisotropy is observed in $\varepsilon_1(0)$ and n(0). In the case of $(MoS_2)_{5L}$–$(WS_2)_{5L}$ and $(MoS_2$–$WS_2)_{5L}$ multilayers, the values of $\varepsilon_1(0)$ and n(0) lie in between the corresponding values for the end arrangements $(MoS_2)_{10L}$ and $(WS_2)_{10L}$. By changing the stacking sequences (AB → AA) values of $\varepsilon_1(0)$ and n(0) increases significantly. This variation in $\varepsilon_1(0)$ and n(0) with stacking configuration may be useful in fabrication of wide range of optoelectronic devices for a variety of applications. This variation in the $\varepsilon_1(0)$ on changing the stacking sequence is in accordance with the Penn model [35]. The Penn model is based on the expression $\varepsilon_1(0) \approx 1 + (\hbar\omega_p/E_g)^2$ where ω_p is the valence electron plasmon frequency and E_g is the band gap. For all the studied multilayers, a change in stacking sequence from AB → AA reduces the band gap which leads to higher values of $\varepsilon_1(0)$ and n(0). The value of $\varepsilon_1(0)$ for bulk MoS_2 is close to the experimental value 17.0 [36] than the earlier theoretical value (12.80) reported by Kumar and Ahluwalia [37].

4. Conclusions

A systematic change in the band gap in MoS_2–WS_2 multilayers along with those of MoS_2 and WS_2 with ten layers is reported by changing the arrangement of layer deposition and stacking configurations. It is found that the indirect band gap within energetically favored AB configuration of MoS_2–WS_2 multilayers changes from 1.07 → 0.97 → 1.22 → 1.29 eV while going from $(MoS_2)_{10L}$ → $(MoS_2)_{5L}$–$(WS_2)_{5L}$ → $(MoS_2$–$WS_2)_{5L}$ → $(WS_2)_{10L}$. The band gap reduces with a change in the stacking from AB to AA. It is also found that the interlayer interaction affects the spacing between S–S atoms and is a key factor in deciding the electronic properties of these multilayers. Optical properties like, absorption coefficients, dielectric tensors, refractive indices, dielectric constants, etc. have also been computed. It is seen that all the studied multilayers show higher values of integrated absorption coefficients of the solar spectrum as compared to bulk Si. Our study predicts that the optoelectronic and photovoltaic properties of MoS_2–WS_2 multilayers can be tuned by changing the stacking configuration and layer deposition arrangement.

Acknowledgements

The authors are thankful to Prof. P. Blaha for Wien2k code. AD is grateful to the Department of Science and Technology (DST), Govt. of India, New Delhi, India for providing financial assistance under Fast Track Young Scientist Project (Grant No.: SR/FTP/PS-063/2011). One of us (UA) is thankful to DST, New Delhi for Junior Research Fellowship (Professional) under INSPIRE program. This work was partially performed at the High Performance Computing Facility at the Inter University Accelerator Centre, New Delhi, India.

References

[1] P.Y. Yu, M. Cardona, Fundamentals of Semiconductors, Springer, New York, 1996.
[2] A.B. Chen, A. Sher, Semiconductor Alloys: Physics and Materials Engineering, Plenum Press, New York, 1995.
[3] Q.H. Wang, K.K. Zadeh, A. Kis, J.N. Coleman, M.S. Strano, Nat. Nanotechnol. 7 (2012) 699–712.
[4] M. Chhowalla, H.S. Shin, G. Eda, L.J. Li, K.P. Loh, H. Zhang, Nat. Chem. 5 (2013) 263–275.
[5] J. Rohrer, P. Hyldgaard, Phys. Rev. B 83 (2011) 165423-1–165423-10.
[6] R. Rao, R. Podila, R. Tsuchikawa, J. Katoch, D. Tishler, A.M. Rao, M. Ishigami, ACS Nano 5 (2011) 1594–1599.
[7] S.B. Kumar, J. Guo, Appl. Phys. Lett. 98 (2011) 222101-1–222101-3.
[8] Y. Kubota, K. Watanabe, O. Tsuda, T. Taniguchi, Science 317 (2007) 932–934.
[9] K.K. Kim, A. Hsu, X. Jia, S.M. Kim, Y. Shi, M. Hofmann, D. Nezich, J.F. Rodriguez-Nieva, M. Dresselhaus, T. Palacios, J. Kong, Nano Lett. 12 (2012) 161–166.
[10] L. Song, L. Ci, H. Lu, P.B. Sorokin, C. Jin, J. Ni, A.G. Kvashnin, D.G. Kvashnin, J. Lou, B.I. Yakobson, P.M. Ajayan, Nano Lett. 10 (2010) 3209–3215.
[11] J. Yan, K.W. Jacobsen, K.S. Thygesen, Phys. Rev. B 86 (2012) 045208-1–045208-11.
[12] E. Kan, H. Ren, F. Wu, Z. Li, R. Lu, C. Xiao, K. Deng, J. Yang, J. Phys. Chem. C 116 (2012) 3142–3146.
[13] G. Gao, W. Gao, E. Cannuccia, J. Taha-Tijerina, L. Balicas, A. Mathkar, T.N. Narayanan, Z. Liu, B.K. Gupta, J. Peng, Y. Yin, A. Rubio, P.M. Ajayan, Nano Lett. 12 (2012) 3518–3525.
[14] C. Lee, H. Yan, L.E. Brus, T.F. Heinz, J. Hone, S. Ryu, ACS Nano 4 (2010) 2695–2700.
[15] T. Korn, S. Heydrich, M. Hirmer, J. Schmutzler, C. Schuller, Appl. Phys. Lett. 99 (2011) 102109-1–102109-3.
[16] S.W. Han, H. Kwon, S.K. Kim, S. Ryu, W.S. Yun, D.H. Kim, J.H. Hwang, J.S. Kang, J. Baik, H.J. Shin, S.C. Hong, Phys. Rev. B 84 (2011) 045409-1–045409-6.
[17] A. Kuc, N. Zibouche, T. Heine, Phys. Rev. B 83 (2011) 245213-1–245213-4.
[18] A. Kumar, P.K. Ahluwalia, Eur. Phys. J. B 85 (2012) 186-1–186-7.
[19] A. Dashora, U. Ahuja, K. Venugopalan, Comput. Mater. Sci. 69 (2013) 216–221.
[20] H. Terrones, F. López-Urías, M. Terrones, Sci. Rep. 3 (2013) 1549-1–1549-7.
[21] J. Kang, S. Tongay, J. Zhou, J. Li, J. Wu, Appl. Phys. Lett. 102 (2013) 012111-1–012111-4.
[22] L. Kou, T. Frauenheim, C. Chen, J. Phys. Chem. Lett. 4 (2013) 1730–1736.
[23] B. Ajalkar, R. Mane, B. Sarwade, P. Bhosale, Sol. Energy Mater. Sol. Cells 81 (2004) 101–110.
[24] H.P. Komsa, A.V. Krasheninnikov, J. Phys. Chem. Lett. 3 (2012) 3652–3656.
[25] C. Lee, J. Hong, M.H. Whangbo, J.H. Shim, Chem. Mater. 25 (2013) 3745–3752.
[26] O. Lopez-Sanchez, D. Lembke, M. Kayci, A. Radenovic, A. Kis, Nat. Nanotechnol. 8 (2013) 497–501.
[27] M. Bernardi, M. Palummo, J.C. Grossman, Nano Lett. 12 (2013) 3664–3670.
[28] P. Blaha, K. Schwartz, G.K.H. Madsen, D. Kvasnicka, J. Luitz, Wien2K Code, An Augmented Plane Wave Plus Local Orbitals Program for Calculating Crystal Properties, Vienna University of Technology, Vienna, Austria, 2012.
[29] F. Tran, P. Blaha, Phys. Rev. Lett. 102 (2009) 226401-1–226401-4.
[30] J.P. Perdew, A. Ruzsinszky, G.I. Csonka, O.A. Vydrov, G.E. Scuseria, L.A. Constantin, X. Zhou, K. Burke, Phys. Rev. Lett. 100 (2008) 136406-1–136406-4.
[31] C.A. Draxl, J.O. Sofo, Comput. Phys. Commun. 175 (2006) 1–14.
[32] K.K. Kam, B.A. ParkInclon, J. Phys. Chem. 86 (1982) 463–467.
[33] P.J. Collings, Am. J. Phys. 48 (1980) 197–199.
[34] http://pveducation.org/pvcdrom/appendicies/standard-solar-spectra.
[35] D.R. Penn, Phys. Rev. 128 (1962) 2093–2097.
[36] A.R. Beal, H.P. Hughes, J. Phys. C: Solid State Phys. 12 (1979) 881–890.
[37] A. Kumar, P.K. Ahluwalia, Physica B 407 (2012) 4627–4634.